Supplement of Atmos. Chem. Phys., 19, 12477–12494, 2019
https://doi.org/10.5194/acp-19-12477-2019-supplement
© Author(s) 2019. This work is distributed under
the Creative Commons Attribution 4.0 License.

Atmospheric Chemistry and Physics
Open Access
EGU

Supplement of

Multivariate statistical air mass classification for the high-alpine observatory at the Zugspitze Mountain, Germany

Armin Sigmund et al.

Correspondence to: Armin Sigmund (armin.sigmund@epfl.ch)

The copyright of individual parts of the supplement might differ from the CC BY 4.0 License.

S1 Atmospheric stability

The range of the pseudo-vertical profile of virtual potential temperature ($\Delta\theta_v$) was almost always positive, indicating stable conditions. In June and July, $\Delta\theta_v$ ranged between -5 K and $+21$ K whereas in December and January, it was generally more positive with values between 4 K and 31 K (Fig. S1a). Upvalley winds at both GAP and ZPLT were generally associated with a less negative $\Delta\theta_v$ compared to downvalley winds, which gave rise to the threshold of 8 K for the distinction between anabatic and katabatic winds (Fig. S1b).

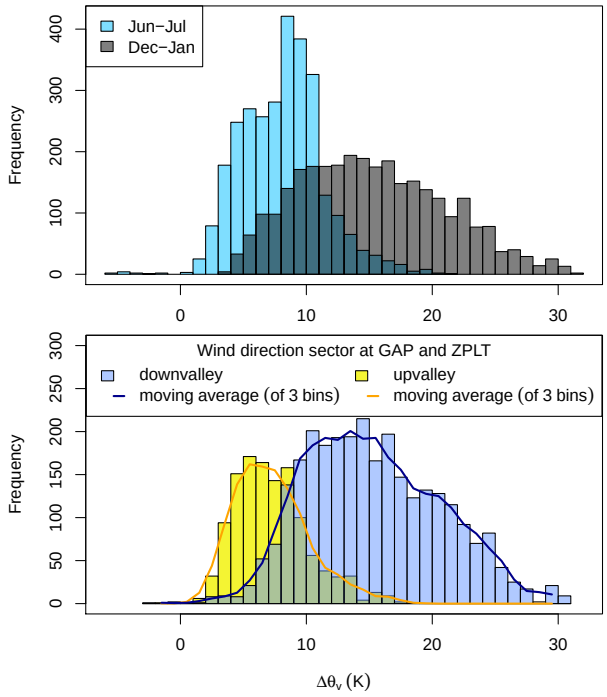

Figure S1. (a) Histograms of the range of the pseudo-vertical profile of virtual potential temperature ($\Delta\theta_v$) for (a) the periods from June to July and from December to January and for (b) upvalley and downvalley wind direction sectors at the stations GAP and ZPLT. Positive values represent stable conditions.

S2 Wind patterns at Zugspitze summit in February and March

Figure S2 shows the wind patterns at ZSG for each of the nine air mass regimes in the 2-month period February–March. The regimes I , II, and III indicated that BL air masses were often associated with southeasterly to southerly winds with varying velocities (Fig. S2a-c). Some of these air masses may reflect south foehn events, especially in the case of strong southerly winds.

For all other regimes, the wind direction was more variable. Strong southerly winds were also included in the regimes IV, V, and VII (Fig. S2d,e,g), which suggests that foehn flows are not always associated with a strong uplift on the windward side of the Alps (Seibert, 1990) and can result in varying air mass characteristics. Regime VII exhibited the highest mean wind velocity (10.22 $\mathrm{m\,s^{-1}}$) among the regimes, which would be in line with a fast transport of the air masses from the marine boundary layer to the UFS (Fig. S2g).

The regimes VIII and IX, which were dominated by UFT/SIN air masses, exhibited similar mean wind velocities compared to the regimes of BL air masses (Fig. S2).

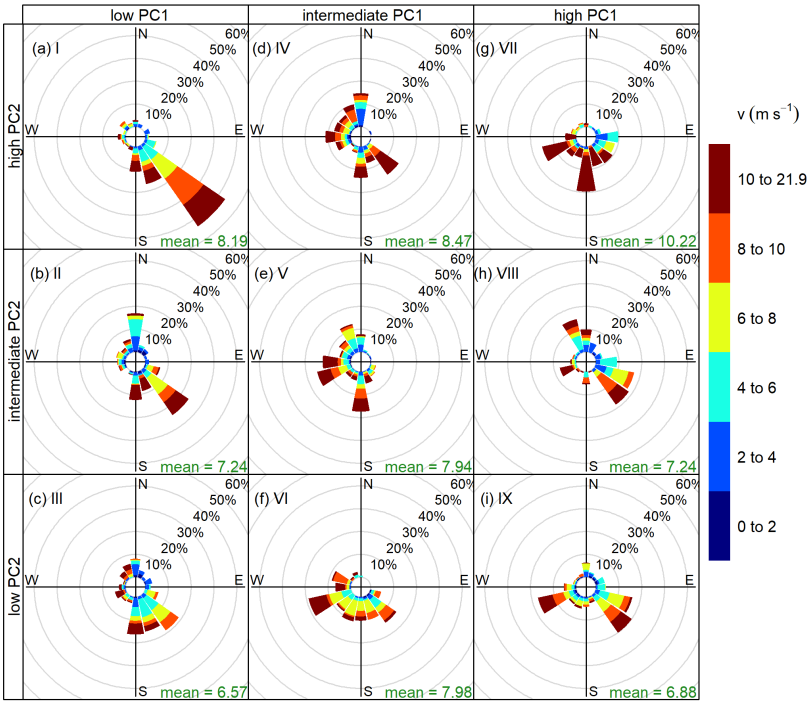

Figure S2. Windrose plots showing the frequency of counts by wind direction and velocity (v) at Zugspitze summit for the nine air mass regimes (I to IX) in February and March 2014. PC1 and PC2 denote the first and second principal components, respectively.

S3 Statistical classification: Case study in March

In a case study, the regimes and classes of air masses were highlighted in the measured time series to gain insight in the transport processes involved and to check the plausibility of the classification. The period from 1 to 13 March 2014 mainly included two phases with contrasting air mass characteristics (Fig. S3). From 1 to 6 March, the three air mass regimes, which were attributed to the class BL, dominated (Fig. S3a) – mainly due to high CO (Fig. S3b), $\mathrm{CH_4}$ (Fig. S3c), and $\mathrm{CO_2}$ mixing ratios (Fig. S3d) that peaked on 5 and 6 March. From 7 to 12 March, the two air mass regimes, which were attributed to the class UFT/SIN in the absence of LRMD, dominated – due to low CO, $\mathrm{CH_4}$, and $\mathrm{CO_2}$ mixing ratios, predominantly low q (Fig. S3e), and high $\mathrm{O_3}$ mixing ratios (Fig. S3f). On 13 March, regime VII indicated ambiguous air masses that originated either from the lower free troposphere or the marine boundary layer (Fig. S3a).

$\Delta\theta_v$ showed weak and strong diurnal variations in the phases from 1 to 6 March and from 7 to 13 March, respectively (Fig. S3g), indicating a shift from cloudy to clear-sky conditions, as confirmed by R_g measurements (Fig. S3s). p_{GAP} reached a minimum on 3 March, increased continuously and strongly until 6 March, and remained high until 13 March (Fig. S3h). These observations suggest that the BL air masses were lifted by a low pressure system and associated fronts whereas the UFT/SIN air masses descended in a high pressure system. This interpretation was supported by high rH (Fig. S3p), precipitation (Fig. S3r), and a low R_g (Fig. S3s) during the strong pressure increase and low rH, absent precipitation and high R_g during the high pressure phase.

The remaining chemical measurements were in line with the classification. $\mathrm{NO_y}$, $\mathrm{NO_x}$ (Fig. S3m), and $^{222}\mathrm{Rn}$ concentrations (Fig. S3n) were substantially higher and $^{7}\mathrm{Be}$ concentrations (Fig. S3o) were much lower for the BL than for the UFT/SIN air masses in the case study. The eBC (Fig. S3j) and N_{90} concentrations (Fig. S3k) tended to be higher for the BL than for the UFT/SIN air masses but temporary wet deposition resulted in strong variations (Fig. S3j,k). The $\mathrm{PM_{10}}$ concentration was only slightly higher for the BL air masses (median of 3.0 $\mu\mathrm{g\,m^{-3}}$) than for the UFT/SIN air masses (median of 2.3 $\mu\mathrm{g\,m^{-3}}$) (Fig. S3i). On 11 March 2014, a stratospheric intrusion was evident from exceptionally high Be-7 (Fig. S3o) and $\mathrm{O_3}$ concentrations (Fig. S3f) of 26 $\mathrm{mBq\,m^{-3}}$ and 79 ppb, respectively, and a low relative humidity of 12 $\%$ (Fig. S3p).

The ceilometer-based MLH at GAP was mostly missing in the period from 1 to 6 March because the uplift of BL air masses was associated with low-level clouds and precipitation (Fig. S3v). From 7 to 12 March, the MLH at GAP mostly showed diurnal variations with afternoon maxima but remained at least 300 m lower than the level of the UFS, which is in line with the statistical classification. Wind direction (Fig. S3t) and velocity (Fig. S3u) at ZSG did not differ significantly between BL and UFT/SIN air masses in the case study.

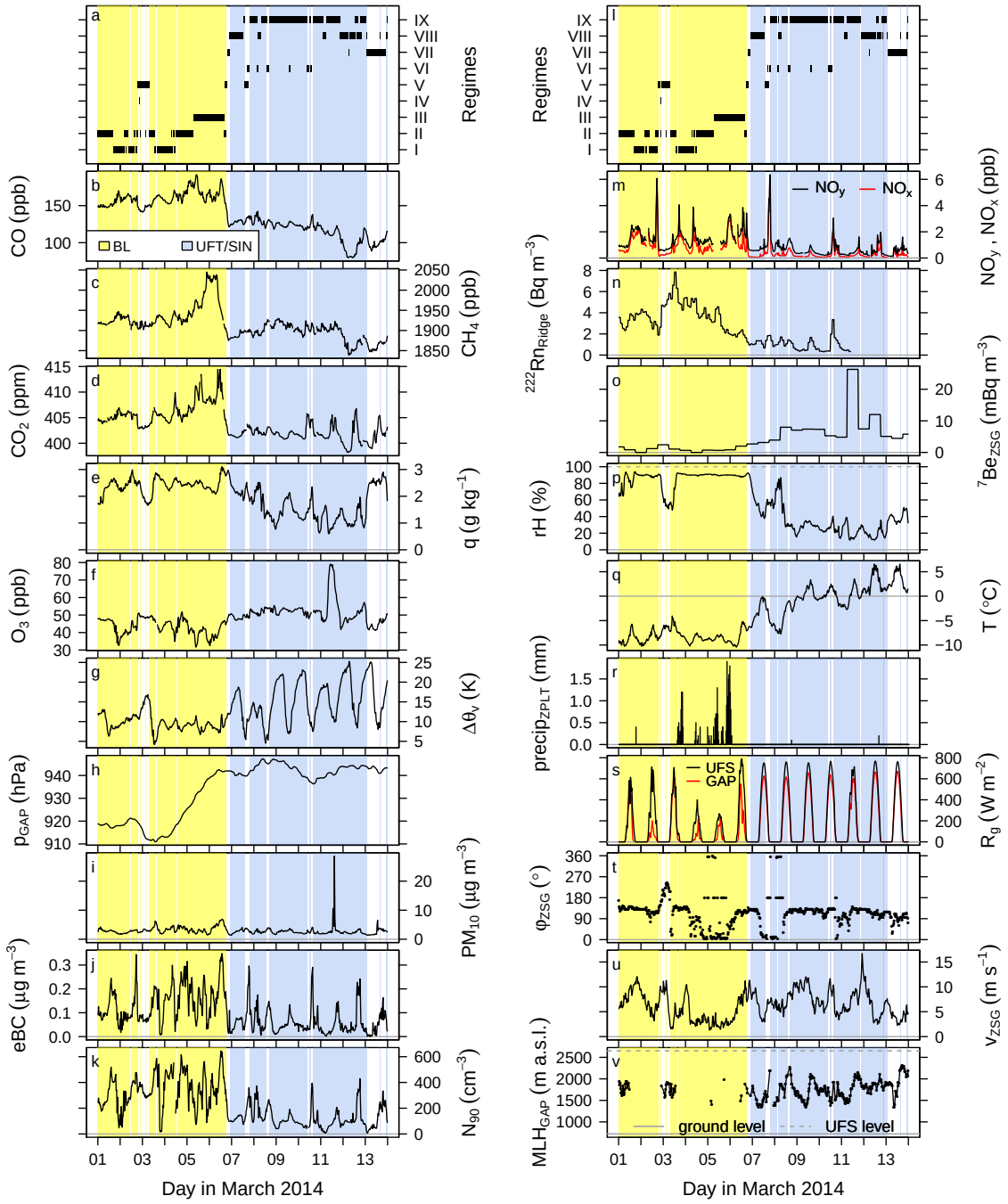

Figure S3. Time series of air mass regimes (a,l), input variables for the classification (b–i), and validation variables (j,k,m–v) from 1 to 13 March 2014. Unless labeled differently, the data was measured at the UFS except for $\Delta\theta_v$ that represents the maximum difference among the sites. The color shading highlights the most important air mass classes. Symbols are explained in Sect. 2.2 and 2.3 of the main article.

References

Seibert, P.: South Foehn Studies Since the ALPEX Experiment, Meteorology and Atmospheric Physics, 43, 91–103, https://doi.org/10.1007/BF01028112, 1990.